DOI: 10.1002/ejic.200901236

Effect of Pore Structure on the Nitridation of Mesoporous Silica with Ammonia

Fumitaka Hayashi,[a] Ken-ichi Ishizu,[a] and Masakazu Iwamoto*[a]

Keywords: Mesoporous materials / Nitrides / Nanostructures / Heterogeneous catalysis / Ceramics

Various mesoporous silicas [MCM-41(M41), SBA-15(SBA15), MCM-48(M48)] and silica gel were nitrided with ammonia in a plug-flow reactor at 1273 K. The nitrogen contents of various (oxy)nitrides obtained were increased with the amount of ammonia supplied per sample weight. The nitridation rates of silica samples were not changed with the pore sizes of the samples but with the pore structures. They were dependent on the surface areas of the parent silicas. The maximum contents of nitrogen in nitrided M41s, SBA15, M48, and silica gel were ca. 38, 35, 39, and 21 wt.-%, respectively, which indicates the great difference between the reactivity of the mesoporous silicas and silica gel. ^{29}Si NMR and X-ray photoelectron spectroscopy also supported the progress in almost complete nitridation of the former samples. The XRD and the FE-SEM measurements revealed that the mesoporous (oxy)nitrides maintained the original 2D hexagonal or 3D cubic mesopore structures and particle morphology. Nitrogen sorption analysis showed that the pore diameters, the surface areas, and the primary mesopore volumes were varied with the nitridation degrees and the types of pore structures but there occurred no destruction of pore structures. Finally, the stabilities of the silicon (oxy)nitrides prepared were studied. The pore structures and nitrogen contents remained essentially unchanged upon storage under a nitrogen atmosphere, immersion in 1-buthanol or toluene, or by heating under H_2 flow at 1073 K. Heating samples under O_2 flow at 1073 K resulted in the collapse of the pore structures and a decrease in nitrogen content.

Introduction

Silicon nitride has attracted much attention because of its high temperature strength, low density, high dielectric constant, and basic properties.[1] Mesoporous silicon nitride (MSN) and oxynitride (MSON) appeared recently as a new class of non-oxide silicon-based mesoporous materials and might have great potential in the fields of catalysis, structural engineering, separation, chemical sensing, and electronics.[2] Recent studies have indeed demonstrated their ability as s solid (super)base,[3–5] host for nanoparticles,[6] and reactive template for nitrogen-incorporated carbon.[7] MSN and MSON are generally prepared by the decomposition of nitrogen-containing silicon compounds[3] or by the replacement of structural oxygen or carbon in mesoporous or mesostructured materials with nitrogen.[4,5,8–16] Previous investigations, however, could not overcome several disadvantages such as the insufficient regularity of the mesopore structure and the low contents of nitrogen.

Very recently, we have developed a new and almost complete nitridation method of M41 with ammonia by using a plug-flow reactor at 1273 K.[16] In the present study, we applied our new preparation method to the nitridation of various mesoporous silicas (MS). The effects of the structural properties on the reaction rate or the maximum nitridation degree were studied in detail. We further compared the structures of the parent mesoporous silicas with those of (oxy)nitrides obtained by using various physicochemical techniques, which confirmed the considerable shrinkage of regular pore structures but their maintenance. At last the stability of mesoporous silicon (oxy)nitrides prepared was studied under a nitrogen atmosphere, in solvents, and under H_2 or O_2 flow at high temperature.

Results and Discussion

Correlation between Pore Structure and Nitridation Reactions

Nitridation Rates of Various MS

We first examined the effect of pore diameter on nitridation by using various M41 samples (p-M41s) with different pore diameters (Table 1, Entries 7, 12, and 16). The reaction conditions and the properties of the M41 samples treated with ammonia (n-M41s) are summarized in Entries 1–6, 9–11, 14, and 15 of Table 1. Figure 1 depicts the dependencies of the nitrogen contents of n-M41s on the total amount of NH_3 supplied at 1273 K. The nitrogen content increased monotonously at 0–2000 $L_{NH_3}g^{-1}$, and it became constant above 2000 $L_{NH_3}g^{-1}$. It should be noted that enough NH_3 was supplied in all experiments because the conversion

[a] Chemical Resources Laboratory, Tokyo Institute of Technology, 4259-R1-5 Nagatsuta, Midori-ku, Yokohama 226-8503, Japan
Fax: +81-45-924-5228
E-mail: iwamoto@res.titech.ac.jp

Supporting information for this article is available on the WWW under http://dx.doi.org/10.1002/ejic.200901236.

levels of NH_3 were always very low (<1.0%). The maximum nitrogen contents were ca. 38 wt.-%, which was very close to 40 wt.-% of Si_3N_4, indicating almost complete nitridation and the presence of a small amount of remaining oxygen.

The figure shows that all of the experimental data on various p-M41s formed an excellent linear correlation line, indicating that the reaction rate of nitridation was independent of the pore size of p-M41. This phenomenon was not varied with the experimental conditions. For example, the nitridation of 1.5 g of M41–16_{CS} (7.5 times greater than those in the usual experiments) in a large plug-flow reactor (inner diameter of 17 mm) gave similar results to those shown in Table 1, Entry 3. This larger-scale experiment also shows easy expansion of the present nitridation method.

The effect of pore structure was then investigated. Figure 2 summarizes the dependencies of the nitrogen contents of n-SBA15, n-M48-16, and n-silica gel on the amount of NH_3 supplied at 1273 K. Firstly, it should be pointed out that the linear correlations between the logarithmic amount of NH_3 supplied and the nitrogen content of n-MSs were again observed on these samples. It should be noted that the slopes of n-SBA15 and n-M48-16 were approximately the same as that of Figure 1. It follows that the nitridation mechanisms of mesoporous silicas would be identical and independent of the pore size or the pore structure. To reveal the reason(s) for the differences among the nitridation rates of various p-MSs, the nitridation degrees at 100 $L_{NH_3}\,g^{-1}$ of NH_3 supplied were plotted against the surface areas of silica samples heated at the nitridation temperature in nitro-

Table 1. Nitridation conditions and properties of parent (p), heated (h), and nitrided (n) MS samples.

Entry	Sample	Nitridation conditions				Nitrogen content	a	D	T	S_{int}		S_{ext}	V		ρ
		Weight / g	t / h	NH_3 flow rate / L min^{-1}	Total NH_3 / L g^{-1}	/ wt.-%	/ nm	/ nm	/ nm	Measd. / m^2 g^{-1}	Theor. / m^2 g^{-1}	/ m^2 g^{-1}	Measd. / mL g^{-1}	Theor. / mL g^{-1}	/ g cm^{-3}
1	n-M41-16_{CS}	0.2	0.25	0.3	22.5	11.7	–[a]	–[b]	–[b]	654	–[b]	92	0.53	–[b]	2.49
2	n-M41-16_{CS}	0.2	1	0.3	90	15.4	3.87	2.92	0.95	576	592	148	0.41	0.42	2.59
3	n-M41-16_{CS}	1.5	4	1	160[c]	21.3	3.91	2.85	1.06	555	501	48	0.34	0.34	2.73
4	n-M41-16_{CS}	0.2	4	0.3	360	27.5	3.90	2.87	1.03	563	487	69	0.33	0.34	2.89
5	n-M41-16_{CS}	0.2	10	0.6	1800	37.9	3.75	2.60	1.15	412	397	138	0.25	0.25	3.15
6	n-M41-16_{CS}	0.2	50	0.8	12000	37.6[d]	3.87	2.55	1.32	303	341	204	0.21	0.21	3.14
7	p-M41-16_{CS}[e]	–	–	–	0	0	4.64	3.81	0.83	826	–	115	0.72	–	2.20
8	h-M41-16_{CS}[f]	0.2	0	0	0	0	4.44	3.57	0.87	758	–	141	0.65	–	2.20
9	n-M41-16_{WG}	0.2	1	0.3	90	16.8	3.78	2.73	0.92	597	573	44	0.34	0.36	2.62
10	n-M41-16_{WG}	0.6	4	0.3	120[c]	19.3	3.74	2.71	1.03	622	573	45	0.34	0.36	2.68
11	n-M41-16_{WG}	0.2	4	0.3	360	27.9	3.68	2.79	0.89	610	613	35	0.38	0.40	2.90
12	p-M41-16_{WG}[e]	–	–	–	0	0	4.57	3.86	0.71	967	–	52	0.83	–	2.20
13	h-M41-16_{WG}[f]	0.2	0	0	0	0	4.49	3.71	0.78	913	–	39	0.74	–	2.20
14	n-M41–22	0.2	1	0.3	90	16.9	4.59	3.39	1.20	482	472	109	0.37	0.38	2.62
15	n-M41–22	0.2	4	0.3	360	25.9	4.46	3.24	1.22	450	427	104	0.32	0.32	2.85
16	p-M41–22[e]	–	–	–	0	0	5.76	4.94	0.82	804	–	223	0.91	–	2.20
17	h-M41–22[f]	0.2	0	0	0	0	5.54	4.73	0.81	804	–	215	0.89	–	2.20
18	n-SBA15	0.2	1	0.3	90	10.9	10.54	8.88	1.66	436	456	55	0.73	0.73	2.47
19	n-SBA15	0.2	4	0.3	360	21.9	10.20	8.63	1.56	406	434	37	0.68	0.68	2.75
20	n-SBA15	0.2	10	0.6	1800	31.0	10.03	8.42	1.61	338	393	72	0.64	0.60	2.98
21	n-SBA15	0.2	20	0.6	3600	35.2	9.88	8.05	1.83	303	339	60	0.60	0.49	3.08
22	n-SBA15	0.2	30	0.6	8100	34.9	9.52	7.72	1.80	298	345	58	0.60	0.48	3.07
23	p-SBA15[e]	–	–	–	0	0	11.66	10.24	1.42	668	–	103	1.02	–	2.20
24	h-SBA15[f]	0.2	0	0	0	0	10.99	9.33	1.66	511	–	87	0.86	–	2.20
25	n-M48–16	0.2	1	0.3	90	17.8	7.64	2.70	1.12	743	723	44	0.45	0.45	2.65
26	n-M48–16	0.2	4	0.3	360	28.6	7.27	2.51	1.10	686	671	46	0.39	0.39	2.92
27	n-M48–16	0.2	10	0.6	1800	34.0	7.27	2.35	1.18	610	598	84	0.33	0.32	3.05
28	n-M48–16	0.2	20	0.6	3600	38.7	7.12	1.95	1.33	408	510	107	0.23	0.23	3.17
29	p-M48-16[e]	–	–	–	0	0	8.59	3.69	0.93	1051	–	65	0.90	–	2.20
30	h-M48-16[f]	0.2	0	0	0	0	8.37	3.21	1.10	887	–	78	0.66	–	2.20
31	n-silica gel	0.2	1	0.3	90	6.1	–	–[a]	–	–[a]	–	–[a]	–[a]	–	2.35
32	n-silica gel	0.2	4	0.3	360	16.0	–	10.4	–	156	–	32	0.47	–	2.60
33	n-silica gel	0.1	8	0.6	2880	20.8	–	–[a]	–	–[a]	–	–[a]	–[a]	–	2.72
34	p-silica gel[e]	–	–	–	0	0	–	11.3	–	215	–	25	0.63	–	2.20
35	h-silica gel[f]	0.2	0	0	0	0	–	10.8	–	149	–	32	0.53	–	2.20

[a] Not measured. [b] Not calculated because of no measurement of the lattice constant using XRD. [c] NH_3 was started to flow onto the sample at 973 K and the sample was heated at 1273 K in NH_3 and treated under the conditions listed in the table. [d] Nitrogen and oxygen contents determined by the nitrogen/oxygen analyzer were 37.8 and 5.7 wt.-%. [e] Parent silica samples. [f] Samples after heating p-MS at 1273 K in a flow of N_2.

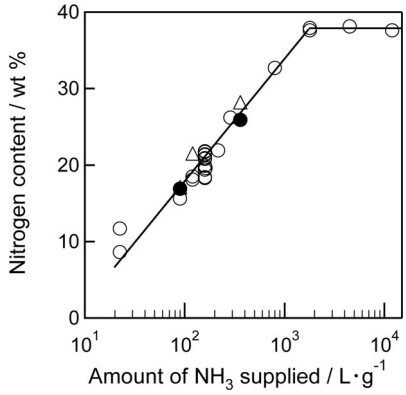

Figure 1. Dependencies of the nitrogen contents of n-M41-16$_{CS}$ (open circle), n-M41-16$_{WG}$ (open triangle), and n-M41-22 (closed circle) on the amount of NH_3 supplied per sample weight at 1273 K.

gen (h-MSs; Entries 8, 13, 17, 24, 30, and 35 in Table 1) in Figure 3. One can observe the very good linear correlation, showing that the reaction rates were determined by surface areas of the parent silicas.

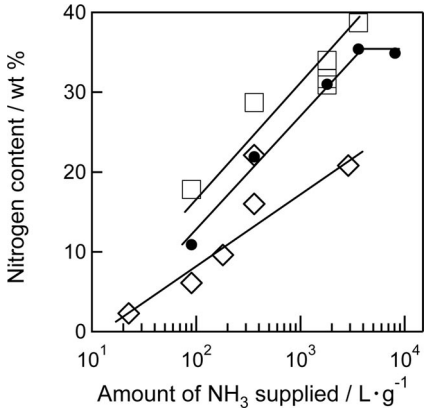

Figure 2. Dependencies of the nitrogen contents of n-SBA15 (closed circle), n-M48-16 (open square), and n-silica gel (open diamond) on the amount of NH_3 supplied per sample weight at 1273 K.

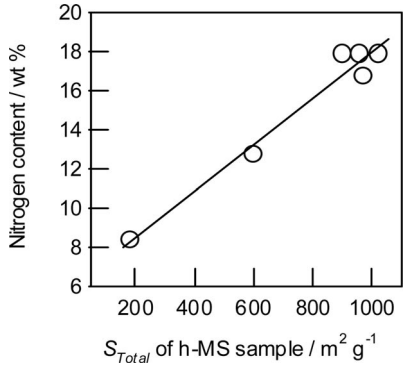

Figure 3. Correlation between the total surface area of h-MS and the nitrogen content of n-MS at 100 $L_{NH_3}\,g^{-1}$.

The second important point in Figures 1 and 2 is that the maximum nitridation degrees of n-M41-16$_{CS}$, n-SBA15, and n-M48-16 were 38, 35, and 39 wt.-%, respectively, at 2000–3600 $L_{NH_3}\,g^{-1}$ and almost the same. It should again be noted that the present preparation method could produce almost pure nitrides. The small amounts of oxygen remaining were supported by the ^{29}Si MAS NMR spectra in Figure 4, which will be described in more detail in the next section. The nitrogen contents of n-MSs determined by ion chromatography were in very good agreement with those by the NMR technique.

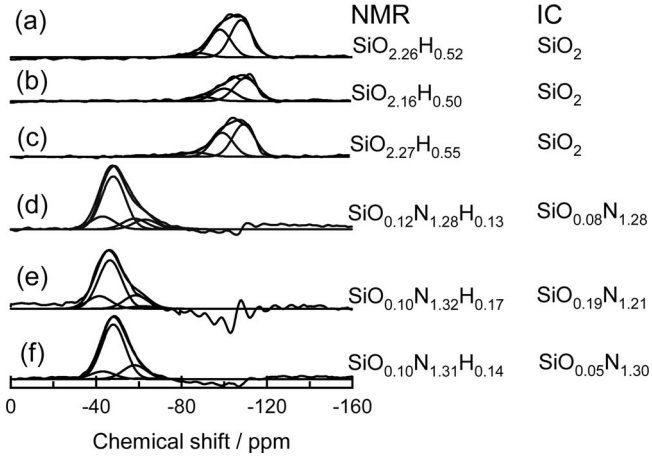

Figure 4. Experimental and deconvoluted ^{29}Si MAS NMR spectra of h-M41-16$_{CS}$ (a), h-SBA15 (b), h-M48-16 (c), n-M41-16$_{CS}$-1800 (d), n-SBA15-3600 (e), and n-M48-16-3600 (f). Spectra (a)–(f) correspond to Entries 8, 24, 30, 5, 21, and 28 in Table 1, respectively. The compositions determined by NMR spectroscopy are shown at the right side together with those obtained by ion chromatography (IC).

Thirdly, the slope of n-silica gel in Figure 2 was lower than those of mesoporous silicas. The increase in the nitrogen content of n-silica gel did not come to the end within the present experiments, which was well consistent with the reports that only high-temperature treatment could achieve deep nitridation of silica.[17–24]

Analysis of the experimental results shown in Figures 1 and 2 was attempted on the basis of various solid-state kinetic models. The rate-determining steps suggested so far could be classified into four groups: the nucleation (A), geometrical contraction (R), diffusion (D), and reaction-order (F) models.[25,26] The following eight models were here adopted: Avrami-Erofeyev model (denoted as A2 in ref.[26]), contracting cylinder model (R2), contracting sphere/cube model (R3), 1D diffusion model (D1), 2D diffusion model (D2), 3D diffusion model (D3), first-order model (F1), and second-order model (F2). The calculated results on the models are summarized in the Supporting Information (Figures S1 and S2) but unfortunately no reaction model could clearly or distinguishably explain the nitridation mechanism.

It is widely recognized that the nitridation of silica with ammonia begins from the surface reactions of silanol and siloxane with ammonia.[17–24] The numbers of silanol and siloxane groups located at the surface are in proportion to the surface areas of the parent silicas. Therefore, the linear

dependence of the reaction rate on the surface area, observed in Figure 3, is reasonable. The wall thicknesses of p-M41s, p-SBA15, p-M48-16, n-M41s, n-SBA15, and n-M48-16 were only 1.0–1.8 nm, which was about one tenth of the particle diameter of h-silica gel (17.2 nm, Supporting Information), and corresponded to only 3–6 layers of O–Si–O (0.26 nm in β-cristobalite[27]) and N–Si–N (0.28 nm in β-Si_3N_4[1]). The very thin walls led us to the speculation that the diffusion of active NH_x species nor water produced by the reaction would not be the rate-determining step of the nitridation.

Characterization of Si, O, and N Species with NMR and XPS

The changes in NMR spectra of Si species with the nitridation degree were already reported.[16] The technique and the assignment were applied here to analyze the present samples. The results are summarized in Figure 4. Spectra d, e, and f showed that the n-M41-16$_{CS}$-1800, n-SBA15-3600, and n-M48-16-3600 samples contained small amounts of oxygen and amide and imide groups as nitrogen species. The respective compositions were evaluated on the assignments and summarized in the figure.

The nitrogen species in n-M41 was then investigated with X-ray photoelectron (XP) spectroscopy. The XP spectra of N 1s, Si 2p, and O 1s of p-M41-16$_{CS}$, n-M41-16$_{CS}$-22.5, n-M41-16$_{CS}$-1800, and crystalline Si_3N_4 are shown in Figure 5 and in the Supporting Information. The reported peak positions[28] of N 1s, Si 2p, and O 1s signals are summarized in the Supporting Information together with the values in the present study. The N 1s spectra will first be discussed. The spectra of n-M41-16$_{CS}$-22.5 and n-M41-16$_{CS}$-1800 could be deconvoluted into three species, respectively. The former, low-nitrided sample, contained the NH$_2$(-SiO$_3$), NH(-SiO$_3$)$_2$, and N(-SiO$_3$)$_3$ species at 399.7, 399.2, and 398.3 eV, respectively, whereas the latter, highly nitrided sample had NH$_2$(-SiN$_3$), NH(-SiN$_3$)$_2$, and N(-SiN$_3$)$_3$ species at 398.6, 398.0, and 397.5 eV, respectively, where the nitrogen atoms corresponding to the XP signals are *italicized*. The presence of the amide and imide groups as well as the nitride species in n-M41-16$_{CS}$-1800 was in excellent agreement with NMR spectroscopic results (Figure 4). It should further be noted that the respective full-widths at half-maxima (FWHM) of the deconvoluted N 1s components of these two samples were all 2.3 eV (Figure 5b,c), which were wider than those of crystalline or amorphous (oxy)nitrides in Figure 5d (1.6 eV) and Supporting Information (1.2–1.8 eV). The results suggest divergences in bond lengths or angles of the respective N species.

The binding energies of Si 2p were shifted from 103.7 eV of SiO_4 species to 101.7 of SiN_4. The shifts were consistent with those of various SiO_xN_y samples reported so far, as shown in the Supporting Information. The n-M41-16$_{CS}$-1800 sample or crystalline Si_3N_4 gave a small signal of O 1s at 532.3 or 532.5 eV, which were very close to 533.1 of O(-SiO$_3$)$_2$ species and 532.2 of O(-SiN$_3$)$_2$ (Supporting Information). The observation of oxygen XP spectra on crystalline Si_3N_4 was widely reported[28c–28e] due to the partial oxidation of crystalline Si_3N_4 surface. At the present we could not distinguish which XP spectra of O 1s observed on n-M41-16$_{CS}$-1800 resulted from unreacted oxygen or from surface oxygen yielded through the oxidation.

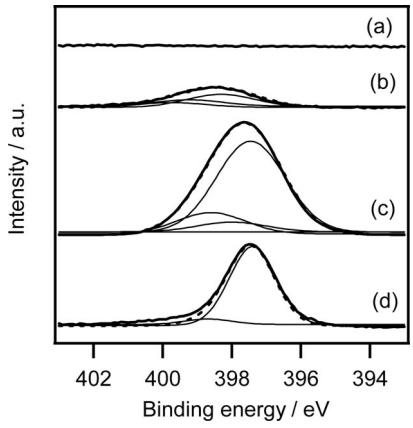

Figure 5. N 1s photoelectron spectra of p-M41-16 (a), n-M41-16$_{CS}$-22.5 (b), n-M41-16$_{CS}$-1800 (c), and crystalline Si_3N_4 (d). Spectra (a)–(c) corresponds to Entries 7, 1, and 5 in Table 1, respectively.

Structural Change through Nitridation

Confirmation of Regular Pore Structures After Nitridation

The changes in the XRD patterns of n-MSs with nitridation treatment are shown in Figure 6 and the Supporting Information. All p-, h-, and n-MSs exhibited well-resolved three peaks assignable to (100), (110), and (200) diffractions of 2D hexagonal *p6 mm* space group (Supporting Information) or eight peaks to (211), (220), (310), (321), (400), (420), (332), and (422) diffractions of 3D bicontinuous cubic *Ia3d* (Figure 6). The intensity of each diffraction decreased with the progress in nitridation. All peaks were shifted to the respective higher angles upon heat or ammonia treatment, which indicated a decrease in the lattice constant and agreed well with the changes observed in the pre-

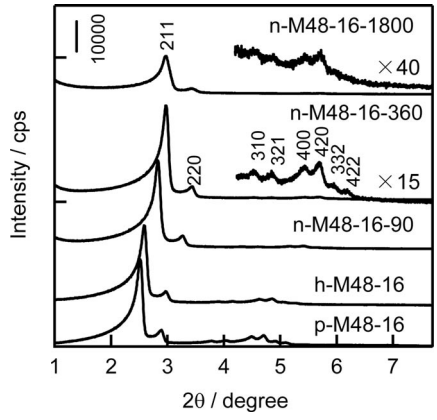

Figure 6. XRD patterns of p-, h-M48-16, n-M48-16-90, -360, and -1800. Patterns correspond to Entries 29, 30, and 25–27 in Table 1, respectively.

vious studies.[4,10–16] No observation of diffraction peaks in the range of 10–60° indicated the presence/maintenance of amorphous oxynitrides walls.

Figure 7 shows the high-resolution FE-SEM images of p-SBA15 and n-SBA15-3600 as typical examples. The particle of p-SBA15 had cylinder-like morphology and the regular array of uniform channels (Figure 7a), which was similar to those of the reported SBA15.[29] As shown in Figure 7b,c, the morphology and the straight and U-shaped pores were kept even after ammonia treatment for 20 h (Table 1, Entry 21). The average diameter and length of the cylinder-like particles of n-SBA15-3600 were 300 and 690 nm, which were 93 and 85% of those of p-SBA15. The shrinkage degrees were in good agreement with those evaluated from the XRD data, which will be discussed in more detail in the latter section. The particles of p-M48-16 were spherical and their sizes were reduced upon ammonia treatment (Figure 7d–f). For example, the average particle diameters of p-M48-16 and n-M48-16-3600 were 565 and 430 nm. The morphology and pore structures of p-M48-16 were maintained after nitridation, which was in contrast to the previous observation[4] that the particles were bunched together during nitridation.

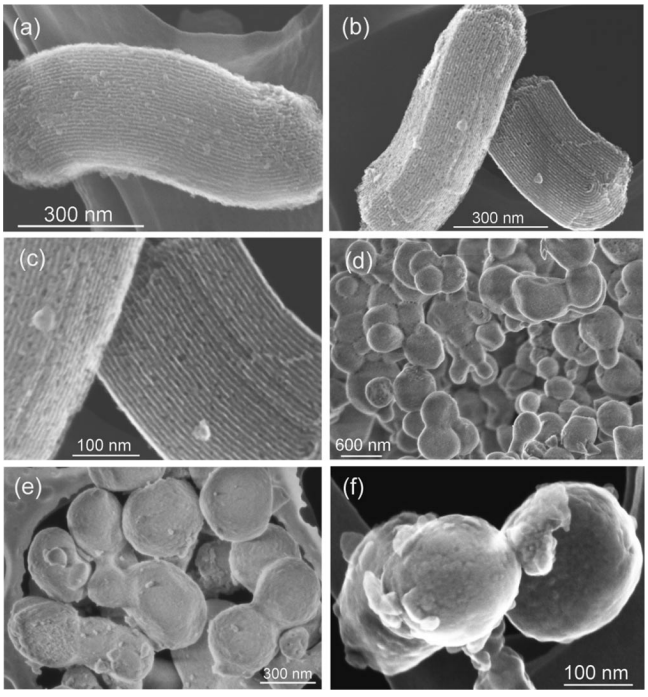

Figure 7. FE-SEM images of p-SBA15 (a), n-SBA15-3600 (b, c), p-M48-16 (d), and n-M48-16-3600 (e, f). Images correspond to Entries 23, 21, 29, and 28 in Table 1, respectively.

The nitrogen adsorption isotherms of various n-MSs are shown in the Supporting Information. The isotherms were of typical type IV curves. Upon nitridation treatment, the steps of the capillary condensation were shifted to the lower pressure ranges and the pore volumes of the respective n-MSs decreased, indicating the shrinkage of pores. The changes in S_{int}, V, D, and T are summarized in Figure 8 as a function of the nitridation degree. The values of p- and h-MSs are also plotted in the figure. It should be added that the linear extrapolation from zero point in the α_s-plots on h- and n-SBA15s revealed no remaining micropores in the samples. The correlations among the structural parameters of n-MSs will be discussed in the next section.

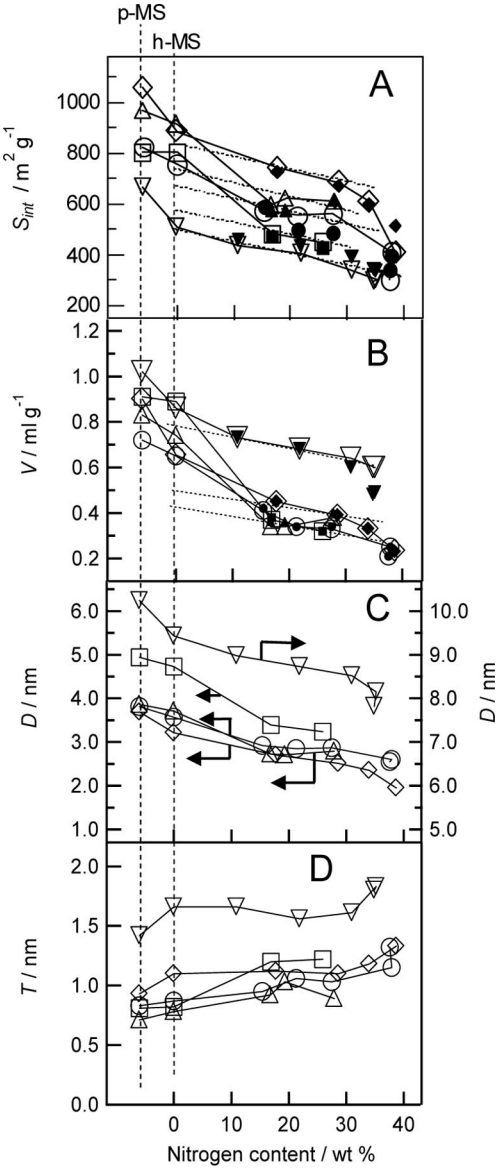

Figure 8. Changes in internal surface area S_{int} (A), mesopore volume V (B), pore diameter D (C), and wall thickness T (D) of n-MS with nitridation degree. Open symbols, experimental values; closed symbols, theoretical values. Circle, n-M41-16$_{CS}$; triangle, n-M41-16$_{WG}$; square, n-M41-22; inverted triangle, n-SBA15; diamond, n-M48-16. Dotted lines; (A) S_{int} = X (ρ_O/ρ_N) (X = 850, 750, 690, 580, and 500), (B) V = Y (ρ_O/ρ_N), (Y = 0.82, 0.50, and 0.43).

Correlations between the Structural Parameters

It has been reported that the decrease in lattice constant a and pore diameter D and the increase in the wall density ρ of M41 through nitridation are due to increments in the number of silicon atoms per 1 nm^3.[16] To confirm the retention of regular pore structures, we calculated the theoretical internal surface areas and mesopore volume of n-MSs on

the assumption of no change in the original 2D hexagonal or 3D cubic pore structure through the present nitridation. The internal surface areas $S_{N,int}$ and mesopore volume V_N of n-MSs can be evaluated by Equations (1) and (2), when those of h-MS were defined as $S_{O,int}$ and V_O.

$S_{N,int}$ = $S_{O,int}$ [(theoretical S_{int} of unit cell of n-MS)/(theoretical weight of unit cell of n-MS)]/[(theoretical S_{int} of unit cell of h-MS)/(theoretical weight of unit cell of h-MS)] (1)

V_N = V_O [(theoretical V of unit cell of n-MS)/(theoretical weight of unit cell of n-MS)]/[(theoretical V of unit cell of h-MS)/(theoretical weight of unit cell of h-MS)] (2)

When the average channel lengths of h- and n-MS are defined as L_O and L_N, Equations (1) and (2) can be converted into Equations (3) and (4) for M41s and SBA15, or into Equations (5) and (6) for M48.[30,31]

$$S_{N,int} = S_{O,int}\{\pi D_N L_N/[(\sqrt{3}/2)a_N^2 - \pi(D_N/2)^2]L_N\rho_N\}/\{\pi D_O L_O/[(\sqrt{3}/2)a_O^2 - \pi(D_O/2)^2]L_O\rho_O\} \quad (3)$$

$$V_N = V_O\{\pi(D_N/2)^2 L_N/[(\sqrt{3}/2)a_N^2 - \pi(D_N/2)^2]L_N\rho_N\}/\{\pi(D_O/2)^2 L_O/[(\sqrt{3}/2)a_O^2 - \pi(D_O/2)^2]L_O\rho_O\} \quad (4)$$

$$S_{N,int} = S_{O,int}\{6.1838a_N^2/[3.0919a_N^3(T_N/a_N)\rho_N]\}/\{6.1838a_O^2/[3.0919a_O^3(T_O/a_O)\rho_O]\} \quad (5)$$

$$V_N = V_O\{a_N^3(3.0919D_N/2a_N)/[3.0919a_N^3(T_N/a_N)\rho_N]\}/\{a_O^3(3.0919D_O/2a_O)/[3.0919a_O^3(T_O/a_O)\rho_O]\} \quad (6)$$

where the subscripts O and N indicate the respective values of h- and n-MS samples. Equations (3), (4), (5), and (6) can be simplified into Equations (7), (8), (9), and (10), respectively.

$$S_{N,int} = S_{O,int}(D_N/D_O)(\rho_O/\rho_N)(2\sqrt{3}a_O^2 - \pi D_O^2)/(2\sqrt{3}a_N^2 - \pi D_N^2) \quad (7)$$

$$V_N = V_O(D_N/D_O)^2(\rho_O/\rho_N)(2\sqrt{3}a_O^2 - \pi D_O^2)/(2\sqrt{3}a_N^2 - \pi D_N^2) \quad (8)$$

$$S_{N,int} = S_{O,int}(T_O/T_N)(\rho_O/\rho_N) \quad (9)$$

$$V_N = V_O(T_O/T_N)(D_N/D_O)(\rho_O/\rho_N) \quad (10)$$

The results of the calculations are summarized in Table 1 as the theoretical S_{int} and V. The values of experimental and theoretical S_{int} and V are compared in Figure 8 as a function of the nitrogen content.

One can point out three correlations in Table 1 and Figure 8. Firstly, the change in the experimental values of S_{int} for all n-MSs with nitridation could be divided into three portions. At the initial stage, the S_{int} values decreased drastically to a greater or lesser degree. At 10–35 wt.-% of nitrogen, the S_{int} values of all n-MSs decreased at roughly fixed rates with the progress in nitridation. Around 39 wt.-%, the change became drastic again. Secondly, the decrease in the experimental V values were similar to those of the experimental S_{int} values (Figure 8A,B). Thirdly, the theoretical S_{int} and V values of all n-MS were in good agreement with the experimental ones, indicating the accuracy of the values of measured a, D, and T and evaluated ρ, and no essential loss of the regular pore structures through nitridation.

The phenomena observed above will be discussed from the changes in structural parameters. At the initial stage of nitridation, the T values should be carefully compared (Figure 8D). Those of n-SBA15 and n-M48-16 increased by ca. 10–20% upon treatment of p-MSs to h-MSs (Table 1, Entries 23 and 24 and 29 and 30) and kept roughly constant during the nitridation process. In contrast, those of h-M41s were approximately the same as those of p-M41s and greatly changed during the nitridation process. The reasons for the difference between M41s and SBA15 or M48 remain unknown but it follows that the wall thickness of p-MSs increased upon heat or nitridation treatment and this is the major reason for the change in the S_{int} and V values. At the middle stage, the values of a, D, and T of all n-MSs changed little and only the values of ρ increased with the nitrogen contents, which caused a slow decrease in the values of S_{int} and V. This discussion could be supported by the facts that the experimental values of S_{int} and V were reasonably expressed with the lines S_{int} = X (ρ_O/ρ_N) (X = 850, 750, 690, 580, and 500) and V = Y (ρ_O/ρ_N), (Y = 0.82, 0.50, and 0.43) as shown in Figure 8A,B, where the values of X and Y are the supposed values. Around the upper limit of nitrogen contents, D and T were further changed, and then the values of S_{int} and V dropped again suddenly. The results indicate that the structural changes in the mesoporous silicas through nitridation are essentially identical and independent of the pore size and the pore structures.

Stability and Reactivity

The stability or reactivity of n-MS was examined under various atmospheres. The n-M41-16$_{CS}$-160 sample (Table 1, Entry 3, abbreviated hereafter as n-M41-S) was employed as a representative because it was prepared in large quantities. Table 2 summarizes the treatment conditions and the properties of the resulting samples. The nitrogen content of n-M41-S after storage at room temperature under an atmosphere of N_2 for five months was comparable to that of the starting n-M41-S (Table 2, Entries 1 and 2). Immersion of n-M41-S in 1-butanol or toluene at room temperature for 2 h resulted in a decrease of ca. 10% in the nitrogen content (Table 2, Entries 3 and 4), whereas in water the decrement was ca. 30% (Table 2, Entry 5). Heat treatment under H_2 flow at 1073 K for 3 h caused a reduction of ca. 10% nitrogen (Table 2, Entry 6), in which the formation of ammonia was detected.[32] Similar decrements and ammonia formation were also observed at 673 and 773 K (not shown). The treatment of n-M41-S under O_2 flow at 1073 K for 3 h led to an 88% loss of nitrogen (Table 2, Entry 7), whereas treatment at 873 K resulted in a loss of 40% (Table 2, Entry 8).

The nitrogen contents changed considerably with the various treatments as mentioned above, but the changes in XRD intensities and nitrogen-adsorption data were considerably different from those. Storage under an atmosphere

Table 2. Properties of n-M41-S treated under various conditions.

Entry	Atmosphere	T / K	Time / h	Nitrogen content / wt.-%	Relative intensity of XRD(100) diffraction[a]	a / nm	S_{total} / $m^2 g^{-1}$	D / nm	V / $mL g^{-1}$
1	–[b]	–	–	20.8	100	3.90	602	2.77	0.31
2	N_2	r.t.	3600	20.3	95	3.75	595	2.53	0.26
3	1-BuOH	r.t.	2	17.8	130	3.78	–[c]	–[c]	–[c]
4	toluene	r.t.	2	18.3	91	3.83	–[c]	–[c]	–[c]
5	H_2O	r.t.	2	14.1	32	3.78	547	2.28	0.19
6	H_2	1073	3	18.2	87	3.80	571	2.50	0.24
7	O_2	1073	3	2.4	8	3.91	45	2.24	0.02
8	O_2	873	3	15.6	69	3.90	581	2.72	0.30

[a] The data are the values obtained from the linear correlation lines in Figures 1 and 2. Calculated by subtraction of background from the peak area of (100) diffraction. [b] Note that this is a different sample to that of Table 1, Entry 3. The deviations are within the experimental errors. [c] Not measured.

of N_2 and immersion in 1-butanol or toluene did not result in a decrease in the XRD intensity (Table 2, Entries 1–4), whereas immersion in water markedly reduced the intensity, though the change in surface area was small (Table 2, Entry 5). Heating under H_2 flow at 1073 K for 3 h resulted in small decreases in the XRD intensity and the surface area (Table 2, Entry 6). The FE-SEM image supports the retention of the regular pore structure after treatment under H_2 flow (Figure 9). In contrast, the pore structure was almost lost upon heat treatment under O_2 flow at 1073 K for 3 h (Table 2, Entry 7).

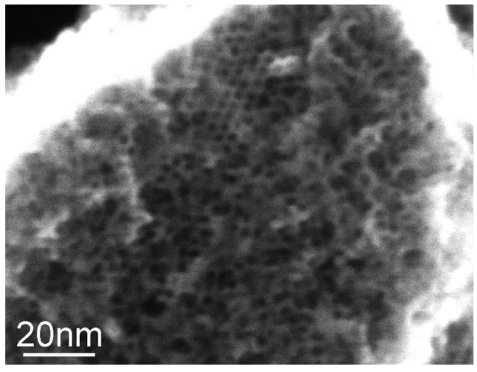

Figure 9. FE-SEM image of n-M41-16_{CS}-160 heated under H_2 flow at 1073 K for 3 h (Table 2, Entry 6).

The stability of nonporous and porous silicon oxynitride was studied by several research groups. Asefa et al. reported that the structural collapse of the nitrided M41 occurred within weeks of storage,[34] whereas Mokaya et al. reported that it did not.[11] It is recognized that nonporous silicon oxynitride prepared at high temperature (1373 K) is of higher stability than that at low temperature (298–398 K).[33,34] The nitridation temperatures in the former[34] and the latter reports[11] were 673–1123 and 1123–1423 K, respectively. The result of the storage in Entry 2 (Table 2) is not consistent with the former but with the latter, which would be due to the nitridation temperature. Two observations should again be pointed out here to discuss the reactivity of the present MSON samples. The NMR and XPS measurements revealed the presence of Si-NH_x species. Their reactivity is reported to be higher than that of nitride N species.[33] In addition, the wider widths of deconvoluted XPS N 1s peaks than those of crystalline materials suggested that N species had various bond lengths and angles in the present samples. The two findings would result in the higher reactivity or the instability of MSON.

The results of immersion in the solvents and heating under H_2 flow indicated that the surface nitrogen species on n-M41 was highly reactive and a certain loss of the nitrogen did not result in the destruction of the pore structure. This property of mesoporous (oxy)nitrides would make it possible for us to apply them in various nitrogen-transfer reactions such as ammonia synthesis because nickel molybdenum nitride[35] and cobalt molybdenum nitride[36] were very recently reported to be active for the reaction. The instability of n-MSs under O_2 flow is due to the difference between the bonding energies of Si–N (355 $kJ mol^{-1}$) and Si–O (452 $kJ mol^{-1}$).[37]

Conclusions

A family of mesoporous silicon (oxy)nitrides was successfully prepared by nitriding various mesoporous silicas with ammonia in a plug-flow reactor at 1273 K. The nitrogen contents were determined by the amount of NH_3 per sample weight, which was independent of the pore size and the pore structure. The reaction rates were determined with the surface areas. The maximum degrees of nitridation were 35–39 wt.-%. Characterization and theoretical calculations revealed the retention of regular pore structures and particle morphology. Because precise control of pore size, pore structure, and particle morphology of mesoporous silica is well established, the use of the present method would enable tailor-made synthesis of mesoporous silicon (oxy)nitrides through the conversion of silica into (oxy)nitride. Unfortunately, the major part of the pore structure and the nitrogen content were lost upon heating under O_2 flow at 1073 K, but were certainly kept during immersion in water, 1-butanol, and toluene and during heating under H_2 flow at 1073 K; these features were also kept under an atmosphere of N_2. The results could lead to potential applications of silicon (oxy)nitrides in various fields of catalysis and adsorption.

Experimental Section

Parent Mesoporous Silicas (p-MSs): The M41-16$_{CS}$, -16$_{WG}$, -22, and SBA15 with 2D hexagonal pore structures (*p6mm*), and M48-16 with 3D cubic structure (*Ia3d*) were prepared according to established procedures,[38–41] where -16 or -22 represents the carbon number of the main chain of surfactant used in the preparation and the subscripts CS and WG mean the employment of colloidal silica and water glass as silica source. Detailed preparation methods are given in the Supporting Information. The structural properties of the p-MSs were determined by various methods described below and are summarized in Table 1, Entries 7, 12, 16, 23, 29, and 34.

Nitridation of p-MSs: Nitridation was carried out in a plug-flow reactor made of quartz (inner diameter, 10 mm). Typically 0.2 g of p-MS was mounted into the reactor, 50 mL/min of N_2 (Japan Air Gases Co., 99.999%) was flowed, and the reactor was heated to 1273 K at a rate of 5 K min^{-1}. Pure NH_3 gas (Japan Air Gases Co., 99.9995%) was introduced into the reactor at the temperature with a NH_3 flow rate of 0.3 or 0.6 L min^{-1} and maintained for a desired time unless otherwise stated. After nitridation treatment, the gas flow was changed to 50 mL min^{-1} of N_2, and then the furnace was cooled to room temperature. The nitrided mesoporous silicas were abbreviated as n-M41–16-A etc., where A is the total amount of NH_3 supplied per sample weight. It has already been revealed that the heating treatment of mesoporous silicas under an atmosphere of N_2 prior to nitridation decreased the pore diameters and surface areas.[16] We therefore prepared heated samples, h-MSs, in separate experiments where p-MS samples were heated at 1273 K under N_2 flow, and the properties of resultant h-MSs are shown in Table 1, Entries 8, 13, 17, 24, 30, and 35.

Characterization: The nitrogen contents of n-MSs were determined by ion chromatography (HIC-10A, Shimadzu Co., Japan) equipped with a CDD-10A conductivity detector or the nitrogen/oxygen analyzer (GMPA 520, Horiba Co., Japan).[15] X-ray diffraction (XRD) patterns were collected by using a Rigaku RINT Ultima$^+$/PC diffractometer with monochromated Cu-K_α radiation. Nitrogen adsorption–desorption isotherms were measured at 77 K with a BEL Japan Belsorp 18 or mini II automatic gas sorption meter after the sample was evacuated at 423 K for 2 h. The Brunauer–Emmett–Teller method was utilized to calculate the specific surface area S_{total}. The external surface area S_{ext} and the primary mesopore volume V were evaluated by using the α_s-plot method.[42] The internal surface area S_{int} was calculated by subtraction of S_{ext} from S_{total}. The pore diameter D of p-, h-, and n-M41s was determined by the Kruk–Jaroniec–Sayari (KJS) method[30] [Equation (11)]. The D of p-SBA15 was determined by Equation (12) because of the existence of a micropore volume V_{micro},[30] whereas h- and n-SBA15 had no micropore and thus Equation (11) could be applied. The D values of p-, h-, and n-M48-16 were determined by Equation (13).[31] The ρ values were estimated by using the correlation between the nitrogen contents and the densities of silicon oxynitrides, which was reported in a previous study.[15] The D values of p-, h-, and n-silica gel were evaluated on the basis of the correlation between the relative pressure of capillary condensation and D.[30] The wall thickness T is calculated by Equation (14) for p-, h-, n-M41s and -SBA15s or Equation (15) for p-, h-, and n-M48s.

$$D = 1.05a[\rho V/(1 + \rho V)]^{1/2} \quad (11)$$

$$D = 1.05a[\rho(V - V_{micro})/(1 + \rho V)]^{1/2} \quad (12)$$

$$D = 2a[\rho V/(1 + \rho V)]/3.0919 \quad (13)$$

$$T = a - D \quad (14)$$

$$T = a/3.0919 - D/2 \quad (15)$$

Solid-state ^{29}Si magic angle spinning nuclear magnetic resonance (MASNMR) spectra were measured with a Bruker AV400M. After various nitridation treatments, the respective samples were transferred from the reactor to a 4-mm pencil-type zirconia-rotor at room temperature under an argon atmosphere. The measurement conditions and the analysis method of the spectra obtained are described in a previous report.[16] Field-emission scanning electron microscopy (FE-SEM) were performed with a Hitachi HR-S5500. X-ray photoelectron spectra were measured with a Shimadzu ESCA 3200. All binding energies were corrected by using the values of C 1s (285.0 eV) or Au 4f$_{7/2}$ (83.8 eV).

Supporting Information (see footnote on the first page of this article): Kinetic analysis using solid-state kinetic models; preparation of p-MSs; XP spectra of p- and n-M41-16$_{CS}$; XRD patterns of p-, h-, and n-MSs; N_2 adsorption isotherms of p-, h-, and n-MSs.

Acknowledgments

The authors thank Prof. Michikazu Hara, Dr. Kiyotaka Nakajima, and Mr. Daigo Adachi of the Tokyo Institute of Technology for XPS measurements. This work was supported in part by Grants-in-Aid from the Ministry of Education, Culture, Sports, Science, and Technology (MEXT) of Japan and the Global COE program of MEXT.

[1] F. L. Riley, *J. Am. Ceram. Soc.* **2000**, *83*, 245.
[2] F. Schüth, *Chem. Mater.* **2001**, *13*, 3184.
[3] S. Kaskel, K. Schlichte, *J. Catal.* **2001**, *201*, 270.
[4] Y. Xia, R. Mokaya, *Angew. Chem. Int. Ed.* **2003**, *42*, 2639.
[5] K. Wan, Q. Liu, C. Zhang, J. Wang, *Bull. Chem. Soc. Jpn.* **2004**, *77*, 1409.
[6] Y. Zhao, Y. Qi, Y. Wei, Y. Zhang, S. Zhang, Y. Yang, Z. Liu, *Microporous Mesoporous Mater.* **2008**, *111*, 300.
[7] J. Wang, Q. Liu, *J. Phys. Chem. C* **2007**, *111*, 7266.
[8] Y. Shi, Y. Wan, B. Tu, D. Zhao, *J. Phys. Chem. C* **2008**, *112*, 112.
[9] M. Wang, Q. Liu, J. Wang, T. Xiu, *J. Am. Ceram. Soc.* **2008**, *91*, 2405.
[10] J. El Haskouri, S. Cabrera, F. Sapina, J. LaTorre, C. Guillem, A. Beltran-Porter, D. Beltran-Porter, M. D. Marcos, P. Amoros, *Adv. Mater.* **2001**, *13*, 192.
[11] Y. Xia, R. Mokaya, *J. Mater. Chem.* **2004**, *14*, 2507.
[12] M. Zhang, Q. Liu, Z. Xu, *J. Non-Cryst. Solids* **2005**, *351*, 1377.
[13] J. Wang, Q. Liu, *Microporous Mesoporous Mater.* **2005**, *83*, 225.
[14] N. Chino, T. Okubo, *Microporous Mesoporous Mater.* **2005**, *87*, 15.
[15] K. Ishizu, F. Hayashi, M. Iwamoto, *Chem. Lett.* **2007**, *36*, 1416.
[16] F. Hayashi, K. Ishizu, M. Iwamoto, *J. Am. Ceram. Soc.* **2010**, *93*, 104.
[17] H. O. Mulfinger, *J. Am. Ceram. Soc.* **1966**, *49*, 462.
[18] C. J. Brinker, D. M. Haaland, *J. Am. Ceram. Soc.* **1983**, *66*, 758.
[19] R. Wusirika, *J. Am. Ceram. Soc.* **1990**, *73*, 2926.
[20] C. R. Bickmore, R. M. Laine, *J. Am. Ceram. Soc.* **1996**, *79*, 2865.
[21] P. W. Lednor, R. de Ruiter, *J. Chem. Soc., Chem. Commun.* **1989**, 320.
[22] K. Szaniawska, L. Murawski, R. Pastuszak, M. Walewski, G. Fantozzi, *J. Non-Cryst. Solids* **2001**, *286*, 58.
[23] M. Sekine, S. Katayama, M. Mitomo, *J. Non-Cryst. Solids* **1991**, *134*, 199.
[24] F. H. P. M. Habraken, A. E. T. Kuiper, Y. Tamminga, J. B. Theeten, *J. Appl. Phys.* **1982**, *53*, 6996.
[25] M. E. Brown, D. Dollimore, A. K. Galwey in *Comprehensive Chemical Kinetics* (Eds.: C. H. Bamford, C. F. H. Tipper), Elsevier, Amsterdam, **1980**, vol. 22.

[26] A. Khawam, D. R. Flanagan, *J. Phys. Chem. B* **2006**, *110*, 17315.
[27] M. O'Keefee, B. G. Hyde, *Acta Crystallogr., Sect. B* **1976**, *32*, 2923.
[28] For examples (see also Supporting Information) a) R. K. Brow, C. G. Pantano, *J. Am. Ceram. Soc.* **1987**, *70*, 9; b) R. K. Brow, C. G. Pantano, *J. Am. Ceram. Soc.* **1984**, *67*, C72; c) M. Peuckert, P. Greil, *J. Mater. Sci.* **1987**, *22*, 3717; d) K. Okada, K. Fukuyama, Y. Kameshima, *J. Am. Ceram. Soc.* **1995**, *78*, 2021; e) J. Szepvolgyi, F. L. Riley, I. Mohai, I. Bertoti, E. Gilbart, *J. Mater. Chem.* **1996**, *6*, 1175.
[29] A. H. Janssen, C.-M. Yang, Y. Wang, F. Schüth, A. J. Koster, K. P. de Jong, *J. Phys. Chem. B* **2003**, *107*, 10552.
[30] a) M. Kruk, M. Jaroniec, A. Sayari, *Langmuir* **1997**, *13*, 6267; b) M. Jaroniec, L. A. Solovyov, *Chem. Commun.* **2006**, 2242.
[31] P. I. Ravikovitch, A. V. Neimark, *Langmuir* **2000**, *16*, 2419.
[32] Flowing gases were trapped in 5 mM sulfuric acid solution and the generated ions were analyzed by ion chromatography.
[33] P. W. Lednor, R. de Ruiter in *Inorganic and Metal-Containing Polymeric Materials* (Eds.: J. E. Sheats, C. E. Carraher, C. U. Pittman Jr., M. Zeldin Jr., B. Currell), Plenum Press, New York, **1990**, pp. 187–195.
[34] T. Asefa, M. Kruk, N. Coombs, H. Grondey, M. J. MacLachlan, M. Jaroniec, G. A. Ozin, *J. Am. Chem. Soc.* **2003**, *125*, 11662.
[35] J. S. J. Hargreaves, D. Mckay, *J. Mol. Catal. A* **2009**, *305*, 125.
[36] D. Mckay, D. H. Gregory, J. S. J. Hargreaves, S. M. Hunter, X. Sun, *Chem. Commun.* **2007**, 3051.
[37] T. L. Cottrell in *The Strengths of Chemical Bonds*, 2nd ed., Butterworths, London, **1958**.
[38] T. Sawada, T. Yano, N. Isshiki, T. Isshiki, M. Iwamoto, *Bull. Chem. Soc. Jpn.* **2008**, *81*, 407.
[39] S. Namba, A. Mochizuki, M. Kito, *Stud. Surf. Sci. Catal.* **1998**, *117*, 257.
[40] D. Zhao, Q. Huo, J. Feng, B. F. Chmelka, G. D. Stucky, *J. Am. Chem. Soc.* **1998**, *120*, 6024.
[41] Y. Xia, R. Mokaya, *J. Mater. Chem.* **2003**, *13*, 657.
[42] M. Kruk, M. Jaroniec, A. Sayari, *Chem. Mater.* **1997**, *9*, 2499.

Received: December 22, 2009
Published Online: April 20, 2010

